Int. J. Electrochem. Sci., 13 **(2018)** 10325 – 10338, doi: 10.20964/2018.11.06

International Journal of
ELECTROCHEMICAL
SCIENCE
www.electrochemsci.org

Improved Discharge Performance of Mg-6Al-7Pb Alloy by Microalloying with Ce

Yiping Wu[1], *Zhifeng Wang*[2], *Yu Liu*[1], *Guofeng Li*[1], *Shaohui Xie*[1], *Hui Yu*[2], *Hanqing Xiong*[1,2,*]

[1] Department of Mechanical and Electronic Engineering, Changsha University, Changsha, 410083, China
[2] School of Materials Science and Engineering, Hebei University of Technology, Tianjin, 300130, China
[*]E-mail: xhanqing@163.com

Received: 8 June 2018 / *Accepted:* 20 July 2018 / *Published:* 1 October 2018

Mg-6Al-7Pb (wt.%) alloys with different Ce contents are prepared and their electrochemical discharge performances are measured in this research. Under casting condition, Mg-6Al-7Pb-0.3Ce alloy shows better electrochemical activity than other alloys. Subsequently, the discharge property of Mg-6Al-7Pb-0.3Ce alloy is further enhanced by multi-pass hot rolling. The result is verified by electrochemical tests and morphology observation. Mg_2Pb and Al_4Ce phases are observed, and fine grains are obtained in as-rolled Mg-6Al-7Pb-0.3Ce alloy. For as-rolled Mg-6Al-7Pb-0.3Ce alloy, the increased discharge performance is attributed to the synergistic effect of the dispersive Al_4Ce and Mg_2Pb phases. The Mg-air battery based on as-rolled Mg-6Al-7Pb-0.3Ce alloy supplies higher peak power density (102.7 $mW \cdot cm^{-2}$) than that based on as-rolled Mg-6Al-7Pb anode. Therefore, the as-rolled Mg-6Al-7Pb-0.3Ce alloy is an excellent anode material for Mg-air battery.

Keywords: Magnesium anode; Microalloying; Hot rolling; Microstructure; Discharge performance

1. INTRODUCTION

Mg-based alloys are good anode materials and have been attracted a great interest due to their excellent discharge performance at high current densities [1-3]. Wang et al. initiated the development of electrochemical activation of Mg-Al-Pb alloy, demonstrating a synergistic effect between aluminum and lead elements in Mg-Al-Pb alloy during discharge process [4]. Subsequently, hot rolling, hot extruding and annealing treatment were carried out to promote the discharge property of Mg-Al-Pb alloys [5, 6]. In the previous literature, the content of Al, Pb and Zn in Mg-Al-Pb-Zn alloys was also discussed using a L_9 orthogonal array test, and the result indicated that Mg_2Pb phase plays an important role in the discharge ability of Mg-6Al-7Pb-0.5Zn alloy [7]. Mg-Pb-Zn ternary system was

investigated and calculated [8], which confirmed that Mg_2Pb phase was formed during annealing treatment at 200 °C. Basically, second phases, as cathodic phases which accelerate the galvanic corrosion and facilitate the peeling of corrosion products, are beneficial for improving the discharge activation of Mg-Al-Pb alloys [9, 10]. It has been reported that Ce-containing Mg alloys exhibit the excellent performance in term of electrochemical activity, utilization efficiency and activation time [11, 12]. In addition, the grains of Mg alloys are refined significantly with Ce addition and meanwhile the rolling capability can be enhanced [13, 14]. Accordingly, it is of great interest to research effects of micro-alloying Ce on the discharge property of Mg-Al-Pb alloy.

2. EXPERIMENTAL

Mg-6Al-7Pb and Mg-6Al-7Pb-XCe were prepared in the graphite crucible in a vacuum induction furnace under argon atmosphere. The raw materials used pure Mg (99.99%), pure Al (99.99%), pure Pb (99.99%) and Mg-30%Ce master alloy. Experimental alloys were molten at 720 °C and held for 10 min. Then, alloy ingots were obtained by casting into a steel mold (200×120×20 mm). With an inductively coupled plasma atomic emission spectrometry (ICP-AES), the compositions (wt.%) of experimental alloys are listed in Table 1. After homogenizing treatment at 420 °C for 24 h, as-cast alloy ingots were quenched in water. The sheets with a thickness of 2 mm were obtained after multi-pass hot rolling at 400 °C and the rolling reduction for every pass was 20%.

Table 1. Chemical composition of experimental alloys under the cast condition.

Alloys	Al	Pb	Ce	Mg
Mg-6Al-7Pb	6.01	6.81	-	Remainder
Mg-6Al-7Pb-0.1Ce	5.98	6.77	0.094	Remainder
Mg-6Al-7Pb-0.3Ce	5.94	6.85	0.291	Remainder
Mg-6Al-7Pb-0.5Ce	5.98	6.76	0.493	Remainder
Mg-6Al-7Pb-0.7Ce	6.02	6.83	0.686	Remainder

As-cast experimental alloys and as-rolled alloys were used for the microstructure observation and electrochemical tests. For the as-rolled alloys, the examination was conducted along the rolling plane. Microstructure was observed by optical microscope (OM), scanning electron microscopy (SEM, Quanta-200) with an energy dispersive spectrometer (EDS), electron probe micro-analysis (EPMA, JXA-8230) and transmission electron microscopy (TEM). The specimens for OM, SEM and EPMA were grinded with metallographic sandpapers (200, 400, 600, 800 and 1200 grit), and then polished with abrasive paste (0.5 μm). A twin-jet electropolishing (TenuPol-5) device was utilized for preparing TEM samples at -20 °C and the electrolyte was comprised of 60% methyl alcohol, 30% glycerin and 10% nitric acid. Before TEM observation, the samples were ion-milled using an ion beam device (Gantan 691). The electrochemical tests were carried out at 25 °C using a Solartron SI 1287 potentiostat/galvanostat system. The three-electrode system was used during test processes, the working electrode was the experimental alloys, the counter electrode was a platinum plate (4 cm × 4

cm), the reference electrode used a saturated calomel electrode (SCE). Before the electrochemical testing, all specimens were polished with the metallographic sandpaper (1000 grit) and a surface of 10 mm × 10 mm was exposed to the electrolyte, and 3.5% NaCl solution served as the experimental electrolyte. Potentiodynamic polarization curves were obtained from -1.90 to -1.20 V with a scan rate of 1 mV^{-1}. For investigating the corrosion properties of as-cast experimental alloys, immersion tests were carried out in the NaCl solution and the hydrogen evolution volume was recorded for 12 h. The galvanostatic discharge test was performed at current densities of 10 or 200 $mAcm^{-2}$ for 1200 s. The impedance spectra (EIS) were recorded at the OCP with 5 mV perturbation amplitude from 100 kHz to 0.1 Hz and the specimen was immersed in electrolyte for 10 min before the test. Anodic efficiencies of experimental alloys were calculated according to mass loss (M_a, g) before and after discharge tests [9], as following relation:

$$\eta = \frac{M_t}{M_a} \times 100\% \qquad (1)$$

In this equation, η represents the anodic efficiency (%). According to the impressed current and the molar mass of alloy elements, the theoretical mass loss (M_t, g) is obtained using Faraday's Law [16].

Fig. 1 shows the schematic of a laboratory Mg-air battery, the cathode is an air electrode using nickel foam as the current collector and MnO_2 as the catalyst [15]. The 4 cm^2 experimental alloy sheets served as anodes for Mg-air battery, and the electrolyte is also 3.5% NaCl solution. Neware battery tester (GT-3008-5V3A-164) was used to evaluate the discharge performance of Mg-air battery. After galvanostatic discharge at different current densities for 10 min, voltage-current curves and power density-current curves were obtained for comparing the discharge performance of different alloy anodes.

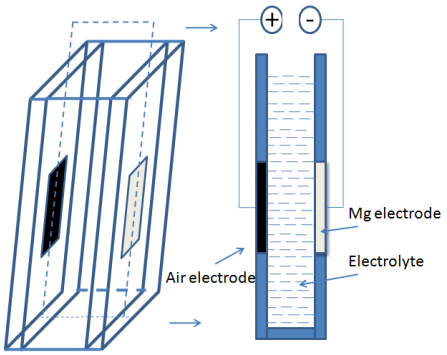

Figure 1. The schematic of a laboratory Mg-air battery.

3. RESULTS AND DISCUSSION

3.1 Microstructure and electrochemical property of as-cast experimental alloys

3.1.1 Microstructure

Fig.2 provides SEM micrographs of as-cast Mg-6Al-7Pb alloys with different Ce contents. In as-cast Mg-6Al-7Pb alloy, β-$Mg_{17}Al_{12}$ phases are observed as remarked in Fig. 1a, and Pb element

exists in the alloy matrix in the form of solid solution because its high sold solubility in Mg matrix [6]. In Fig.2b, white particles are found in the Mg-6Al-7Pb-0.1Ce alloy. With the increase of Ce content, the volume fraction of white particles increases as plotted in Fig.2c, d and e. In Fig.2d, the shape of white particle is revealed in the inset image. The chemical constituent of the white particle is analyzed by EPMA, indicating that the particle contains 55.4531 at.% Mg, 36.0318 at.% Al, 0.2062 at.% Pb and 8.3089 at.% Ce. The atom ratio of Al/Ce is about 4:1 for the particle which is identified as Al_4Ce phase [14, 17].

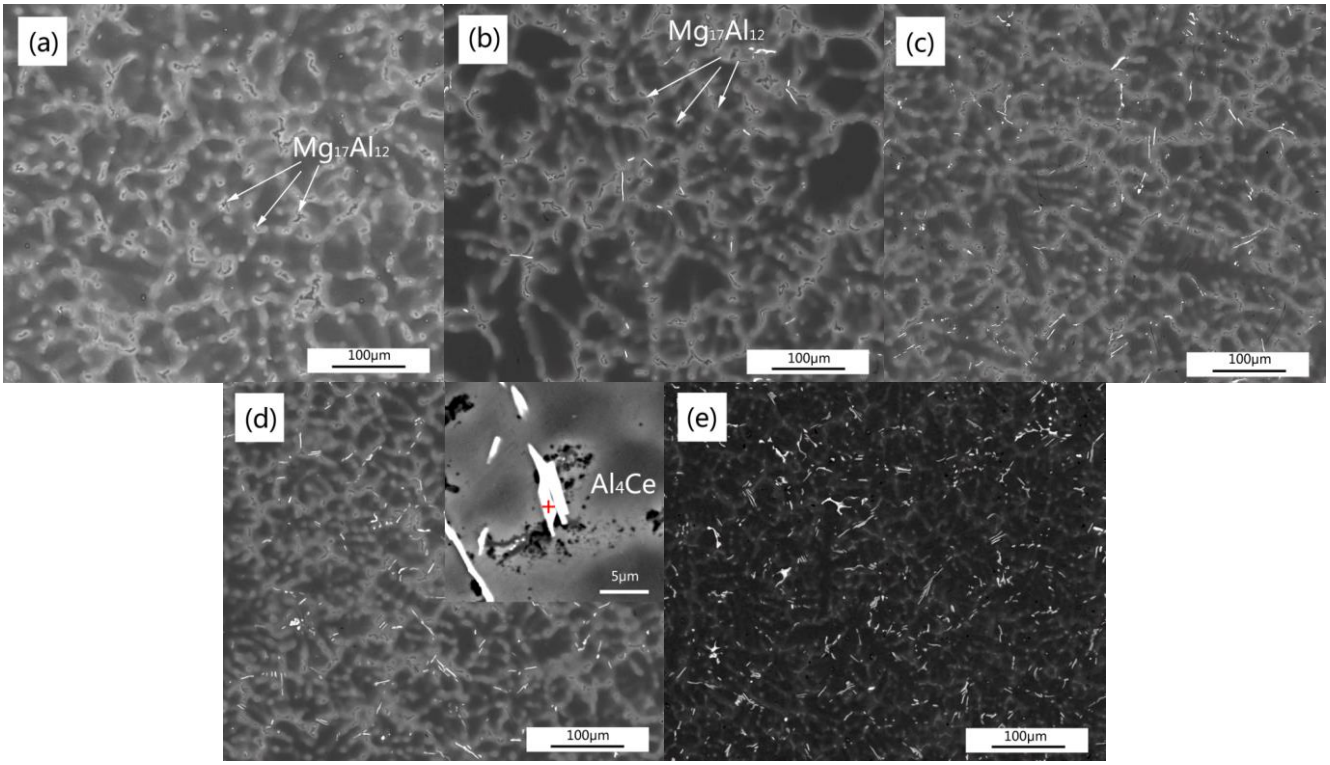

Figure 2. SEM micrographs of as-cast Mg-6Al-7Pb alloys with different Ce contents. (a) Mg-6Al-7Pb alloy, (b) Mg-6Al-7Pb-0.1Ce alloy, (c) Mg-6Al-7Pb-0.3Ce alloy, (d) Mg-6Al-7Pb-0.5Ce alloy and (e) Mg-6Al-7Pb-0.1Ce alloy.

3.1.2 Electrochemical property

Fig. 3 shows polarization curves of as-cast Mg-6Al-7Pb and Mg-6Al-7Pb-XCe alloys in 3.5% NaCl solution, and corrosion parameters are listed in Table 2. It is obvious that the corrosion potential (E_{corr}) of as-cast Mg-6Al-7Pb-XCe alloys is firstly shifted toward negative direction with the increase of Ce content, while the E_{corr} is then toward positive direction when the content of Ce element is more than 0.3%. For Mg alloys, the cathodic polarization curve is related to the water reduction ($2H_2O + 2e \rightarrow H_2 + 2OH^-$) in aqueous solution [18]. Thus, the corrosion current densities of experimental alloys can be obtained by Tafel extrapolation in the cathodic branches [19]. The corrosion current (J_{corr}) of as-cast Mg-6Al-7Pb-XCe alloys is firstly enhanced and then is reduced with the increase of Ce contents. This also means that the corrosion resistance of as-cast Mg-6Al-7Pb-XCe alloys is weakened firstly

and then is strengthened with the increase of Ce content. Moreover, the cathodic kinetics can be reflected by the cathodic Tafel slope (b_c) value which also indicates the hydrogen evolution behavior. A small b_c value means a large cathodic kinetics and high hydrogen evolution rate. Thus, compared with other ones, as-cast Mg-6Al-7Pb-0.3Ce alloy shows higher hydrogen evolution rate in Fig.4. The result of hydrogen evolution test is contrast with the polarization test. Actually, the corrosion resistance of Mg-Al alloys can be enhanced by adding appropriate Ce element which suppresses the precipitation of deleterious β-$Mg_{17}Al_{12}$ phases and instead results in more continuous β-$Mg_{17}Al_{12}$ phases [20]. The anodic branch of magnesium anode can reflect its discharge activity during anodic polarization [6], because the anodic polarization curve represents the dissolution of Mg matrix ($Mg \rightarrow Mg^{2+} + 2e$). Obviously, there are different anodic polarization behaviors for experimental alloys. During the anodic polarization, as-cast Mg-6Al-7Pb-0.3Ce alloy exhibits smaller anodic Tafel slope (b_a) than other ones, meaning that it has stronger discharge activity. Subsequently, the galvanostatic measurements of as-cast experimental alloys are performed at the current density of 200 $mAcm^{-2}$, because the density can be used to evaluate the discharge property of Mg anodes in low or high power applications [15]. The result shows that as-cast Mg-6Al-7Pb-0.3Ce alloy presents more negative discharge potential than other ones, as shown in Fig. 5. Thus, Mg-6Al-7Pb-0.3Ce alloy is selected for the following research.

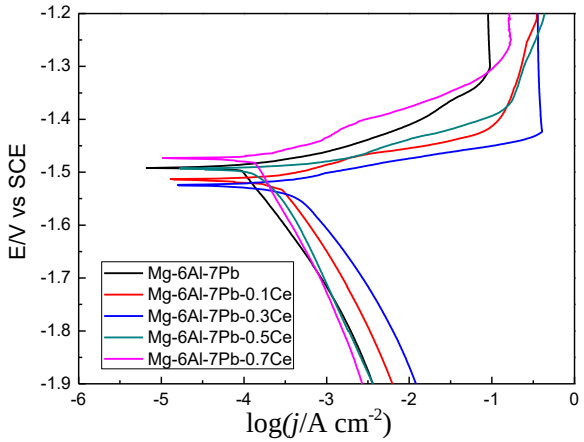

Figure 3. Polarization curves of as-cast Mg-6Al-7Pb and Mg-6Al-7Pb-XCe alloys in 3.5% NaCl solution.

Table 2. Corrosion parameters of as-cast Mg-6Al-7Pb and Mg-6Al-7Pb-XCe alloys in 3.5% NaCl solution.

Alloys	E_{corr} (V vs SCE)	J_{corr} (μA /cm^{-2})	b_c/(mV dec^{-1})	b_a/(mV dec^{-1})
Mg-6Al-7Pb	-1.492	64.84	-169	47
Mg-6Al-7Pb-0.1Ce	-1.513	83.42	-128	42
Mg-6Al-7Pb-0.3Ce	-1.524	102.14	-110	38
Mg-6Al-7Pb-0.5Ce	-1.495	77.78	-155	41
Mg-6Al-7Pb-0.7Ce	-1.473	73.72	-193	51

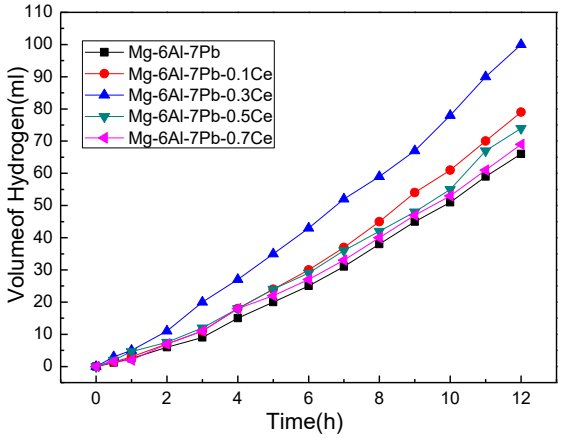

Figure 4. Hydrogen evolution volume of as-cast Mg-6Al-7Pb and Mg-6Al-7Pb-XCe alloys with the increasing time in 3.5% NaCl solution.

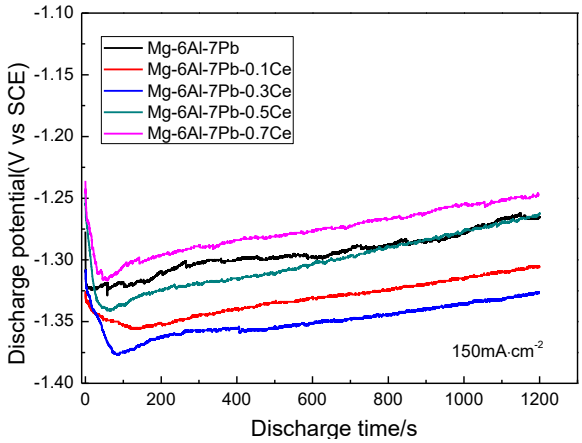

Figure 5. Potential-time curves of as-cast alloys at the anodic current densities of 200 mA·cm^{-2} for 1200 s in 3.5% NaCl solution.

3.2 Microstructure and electrochemical property of as-rolled experimental alloys

3.2.1 Microstructure

Apart from adding alloy elements into Mg matrix, it is confirmed that heat treatment and plastic deformation can enhance the discharge performance due to changing the microstructure of Mg anodes [5, 21]. After homogenization and multi-pass hot rolling, microstructure images of as-rolled Mg-6Al-7Pb and Mg-6Al-7Pb-0.3Ce alloys are shown in Fig. 6. It has been found that as-rolled Mg-6Al-7Pb-0.3Ce alloy has a more uniform microstructure than as-rolled Mg-6Al-7Pb alloy, as shown in Fig. 6a and b. The average size of grains is 25 μm for as-rolled Mg-6Al-7Pb-0.3Ce alloy, while the grain extraordinary growth is presented in as-rolled Mg-6Al-7Pb alloy. Fig. 6c and d show TEM images of as-rolled Mg-6Al-7Pb and Mg-6Al-7Pb-0.3Ce alloys, respectively. In Fig. 6c, fine Mg_2Pb phases are formed in as-rolled Mg-6Al-7Pb alloy, which may originate from the dynamic precipitation during hot rolling and low temperature annealing [7, 8]. The EDS result of zone C in Fig.6d signifies that the particle is Mg_2Pb phase. With the EDS of zone A in Fig. 6d, it indicates the A and B particles are Al_4Ce phase, which still exist after homogenization and rolling [14]. Thus, the addition of Ce promotes the refinement of grains and the formation of uniform microstructure.

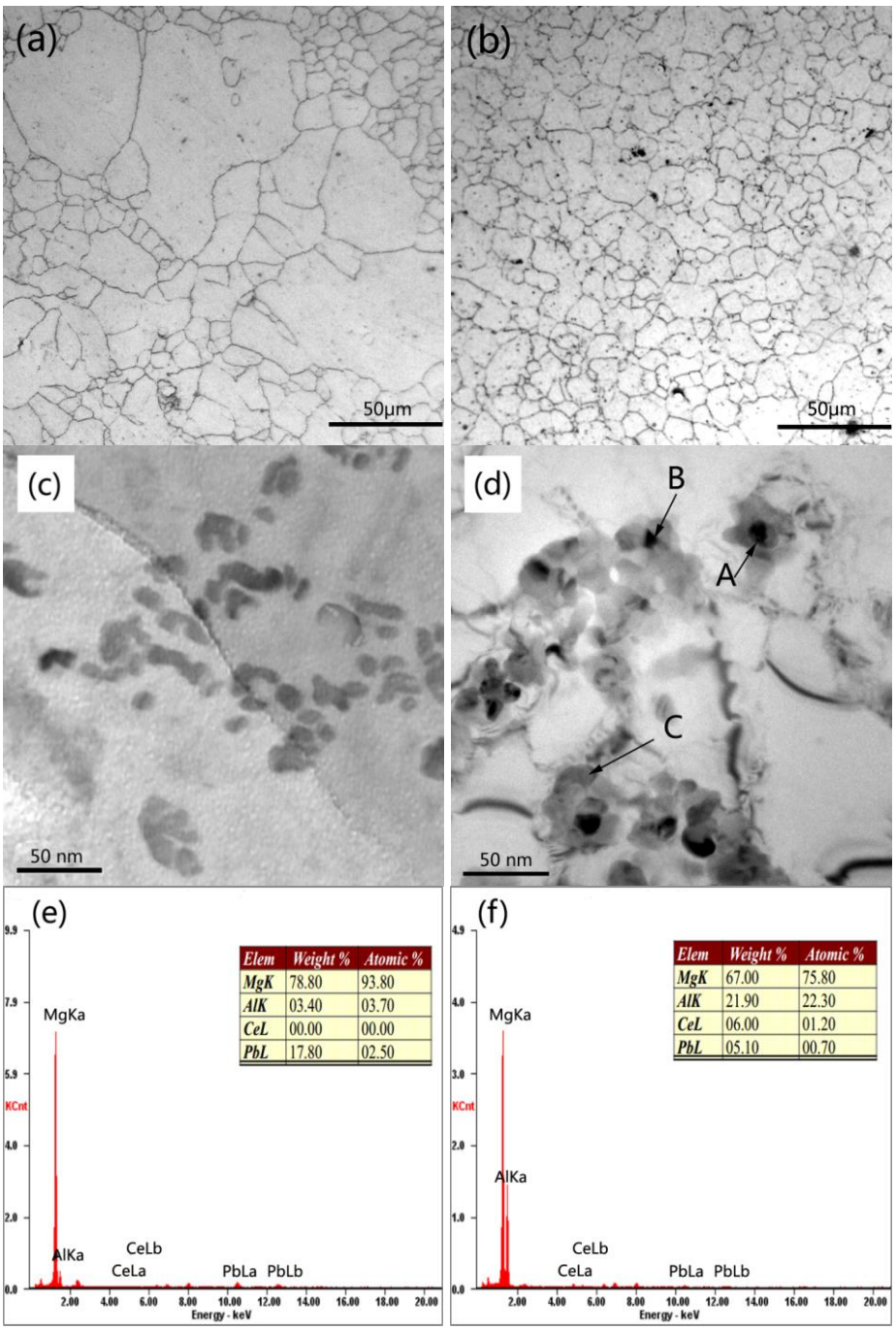

Figure 6. Microstructures of as-rolled Mg-6Al-7Pb and Mg-6Al-7Pb-0.3Ce alloys. OM images of as-rolled Mg-6Al-7Pb alloy (a) and as-rolled Mg-6Al-7Pb-0.3Ce alloy (b), TEM images of as-rolled Mg-6Al-7Pb alloy (c) and as-rolled Mg-6Al-7Pb-0.3Ce alloy (d), EDS images of zone C (e) and zone A (f).

3.2.2 Polarization test

Fig.7 shows polarization curves of as-rolled Mg-6Al-7Pb and Mg-6Al-7Pb-0.3Ce alloys in 3.5% NaCl solution and corresponding corrosion parameters are listed in Table 3. The E_{corr} decreases in the following order: as-cast Mg-6Al-7Pb > as-cast Mg-6Al-7Pb-0.3Ce > as-rolled Mg-6Al-7Pb >

as-rolled Mg-6Al-7Pb-0.3Ce. Thus, the electrochemical activity increases in the following order: as-cast Mg-6Al-7Pb < as-cast Mg-6Al-7Pb-0.3Ce < as-rolled Mg-6Al-7Pb < as-rolled Mg-6Al-7Pb-0.3Ce. Obviously, the electrochemical activity of as-cast alloys is improved after multi-pass hot rolling. This is ascribed to the grain refinement and the increasing grain boundaries after multi-pass hot rolling. The increase of grain boundaries can provide more electrochemical reaction channels [22]. Table 3 also shows that the J_{corr} increases in the following order: as-cast Mg-6Al-7Pb < as-cast Mg-6Al-7Pb-0.3Ce < as-rolled Mg-6Al-7Pb < as-rolled Mg-6Al-7Pb-0.3Ce. Compared with as-cast Mg-6Al-7Pb alloy, as-rolled Mg-6Al-7Pb alloy presents larger J_{corr} because β-$Mg_{17}Al_{12}$ phases are dissolved into Mg matrix. It has been reported that β-$Mg_{17}Al_{12}$ phases are not found in AP65 alloy after hot rolling and heat treatment [6]. In addition, the previous research has not yet found β-$Mg_{17}Al_{12}$ phases in as-rolled Mg-Al-Pb-Zn alloys [7]. This is because the addition of Pb element reduces the diffusion of Mg and Al atoms and consequently the precipitation of β-$Mg_{17}Al_{12}$ phases is inhibited [23]. With β-$Mg_{17}Al_{12}$ phases as corrosion barriers in Mg alloys, the corrosion resistance can be increased. Thus, as-cast alloy exhibits smaller J_{corr} than the other experimental alloys [24]. However, the inhibiting effect of β-$Mg_{17}Al_{12}$ phases is eliminated in as-rolled Mg-6Al-7Pb-0.3Ce alloy. Compared with as-cast Mg-6Al-7Pb-0.3Ce alloy, as-rolled Mg-6Al-7Pb-0.3Ce alloy presents larger J_{corr} and smaller b_c value. For one hand, β-$Mg_{17}Al_{12}$ phases are dissolved into Mg matrix. For the other hand, Al_4Ce phase is remained and Mg_2Pb phase precipitates in as-rolled Mg-6Al-7Pb-0.3Ce alloy. Related researches show that the electrode potential of Al_4Ce or Mg_2Pb is much lower than pure Mg [25, 26], thus the two phases can acts as cathodes to promote the corrosion and dissolution of Mg matrix. As-rolled Mg-6Al-7Pb-0.3Ce alloy presents larger J_{corr} than as-rolled Mg-6Al-7Pb alloy. Furthermore, it is easy to find in Table 3 that as-rolled Mg-6Al-7Pb-0.3Ce alloy exhibits stronger discharge activity and presents larger anodic corrosion current than other ones, according to their b_a values. Table 3 also reveals that as-rolled alloys have stronger discharge activity than as-cast alloys, thus subsequent detailed discussions focus on as-rolled Mg-6Al-7Pb and Mg-6Al-7Pb-0.3Ce alloys.

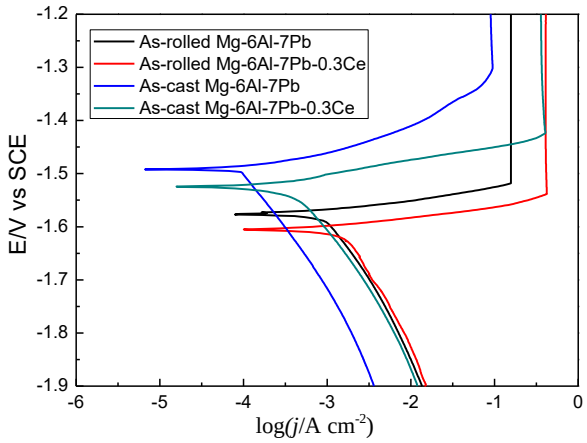

Figure 7. Polarization curves of Mg-6Al-7Pb and Mg-6Al-7Pb-0.3Ce alloys under two conditions in 3.5% NaCl solution.

Table 3. Corrosion parameters of Mg-6Al-7Pb and Mg-6Al-7Pb-0.3Ce alloys under two conditions in 3.5% NaCl solution.

Alloys	E_{corr} (V vs SCE)	J_{corr} (μA /cm^{-2})	b_c/(mV dec^{-1})	b_a/(mV dec^{-1})
As- rolled Mg-6Al-7Pb	-1.576	320.87	-163	36
As-rolled Mg-6Al-7Pb-0.3Ce	-1.606	380.14	-151	32
As-cast Mg-6Al-7Pb	-1.495	64.84	-169	47
As-cast Mg-6Al-7Pb-0.3Ce	-1.524	102.13	-110	38

3.2.3 Galvanostatic discharge test

Different current densities can evaluate different power applications. For Mg-Al-Pb alloy system, it is often considered as the anode for high-power batteries [3]. Thus, the galvanostatic tests of as-rolled Mg-6Al-7Pb and Mg-6Al-7Pb-0.3Ce alloys are carried out at two different current densities, 10 mAcm^{-2} or 200 mAcm^{-2}. Fig. 8 gives potential-time curves and results show that as-rolled Mg-6Al-7Pb-0.3Ce alloy exhibits more negative potential than as-rolled Mg-6Al-7Pb alloy at two different current densities. At the current density of 10 mAcm^{-2}, the average potential of as-rolled Mg-6Al-7Pb-0.3Ce alloy reaches 1.786 V (vs. SCE), while that of as-rolled Mg-6Al-7Pb alloy is 1.728 V (vs. SCE). The average potential of as-rolled Mg-6Al-7Pb-0.3Ce alloy is also higher at the current density of 200 mAcm^{-2}, the average potential is 1.698 V (vs. SCE) for as-rolled Mg-6Al-7Pb-0.3Ce and 1.611 V (vs. SCE) for as-rolled Mg-6Al-7Pb alloy, respectively. With high average discharge voltages, as-rolled Mg-6Al-7Pb-0.3Ce alloy can be a better candidate for anode materials. Moreover, as-rolled Mg-6Al-7Pb-0.3Ce alloy presents a stable discharging process during galvanostatic measurements. After discharge at 200 mAcm^{-2} for 200s, the discharge potential of as-rolled Mg-6Al-7Pb alloy shift to more positive suddenly. As-rolled Mg-6Al-7Pb alloy also shows obvious voltage fluctuation compared with as-rolled Mg-6Al-7Pb-0.3Ce one during discharge at 200 mAcm^{-2}. For as-rolled Mg-6Al-7Pb-0.3Ce alloy, the superior discharge behavior may benefit from the synergistic effect of the dispersive Al_4Ce and Mg_2Pb phases which facilitate the peeling of hydroxide film, because the two phases can act as cathodes to accelerate the corrosion coupling with α-Mg matrix.

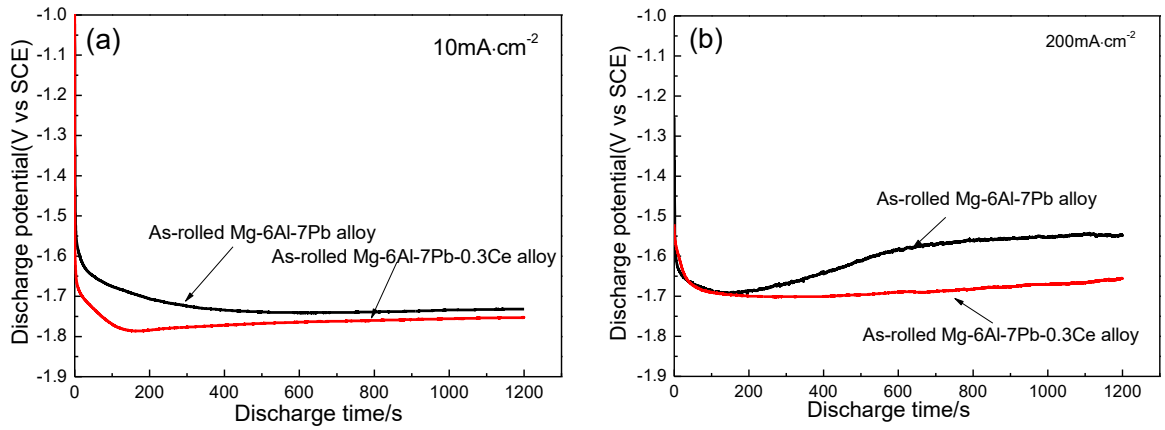

Figure 8. Potential-time curves of as-rolled Mg-6Al-7Pb and Mg-6Al-7Pb-0.3Ce alloys at different current densities in 3.5% NaCl solution.

3.2.4 Electrochemical impedance spectra (EIS)

Fig. 9a shows EIS curves of as-rolled Mg-6Al-7Pb and Mg-6Al-7Pb-0.3Ce alloys in 3.5% NaCl solution after discharge test at 200 mAcm^{-2} for 1200 s. And corresponding equivalent circuits are given in Fig. 9b, in which the constant phase element (CPE) is used to represent the double-layer capacitance. In the plots of two alloys, a capacitive loop is observed in the high frequency region. The capacitive loop indicates the electric double layer (CPE_1) and the charge transfer process (R_t) at the electrode/electrolyte interface [9], implying that the activation-controlled process occurs on the surface of the two alloys [15].

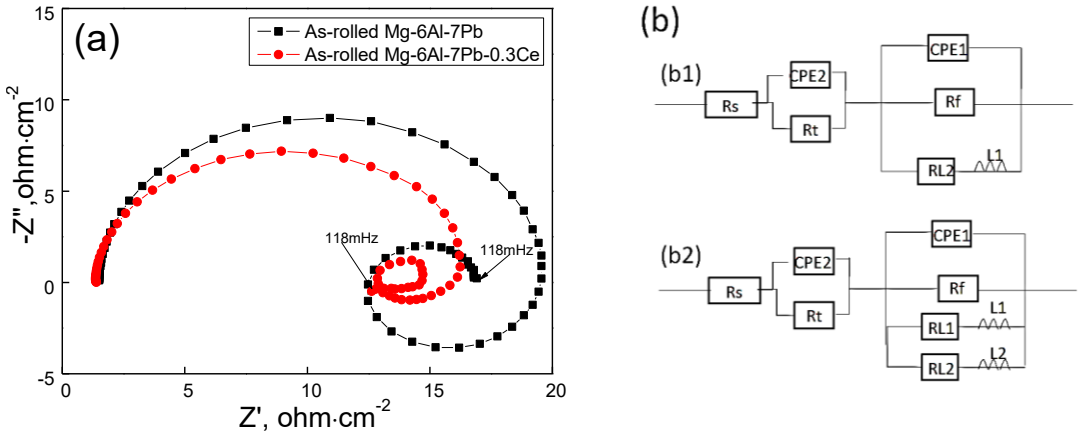

Figure 9. EIS curves of as-rolled Mg-6Al-7Pb and Mg-6Al-7Pb-0.3Ce alloys (a) and equivalent circuit of EIS plots (b) after discharge test at 200 mA·cm^{-2} for 1200 s.

Table 4. EIS simulated values of as-rolled Mg-6Al-7Pb and Mg-6Al-7Pb-0.3Ce alloys after discharge test at 200 mA·cm^{-2} for 1200 s

Alloys	As-rolled Mg-6Al-7Pb	As-rolled Mg-6Al-7Pb-0.3Ce
Rs ($\Omega\cdot cm^2$)	0.894	0.6611
CPE_1 ($\Omega^{-1}\cdot cm^{-2}\cdot s^n$)	1.638×10^{-5}	2.676×10^{-5}
n_1 ($0 < n < 1$)	0.9931	0.9796
R_t ($\Omega\cdot cm^2$)	18.17	14.98
CPE_2 ($\Omega^{-1}\cdot cm^{-2}\cdot s^n$)	0.01208	0.02685
n_2 ($0 < n < 1$)	1	1
R_f ($\Omega\cdot cm^2$)	6.187	2.466
R_{L1} ($\Omega\cdot cm^2$)	18.67	39.9
L1($H\cdot cm^2$)	0.4767	0.5131
R_{L2} ($\Omega\cdot cm^2$)	--	49.8
L2($H\cdot cm^2$)	--	38.49
χ^2	3.151×10^{-4}	1.637×10^{-3}

In the low frequency region, an inductive loop (R_1, L_1) and a small capacitive loop (CPE_2, R_f) are presented in EIS curves of the two alloys, which is regarded as the damage of $Mg(OH)_2$ film and the occurrence of localized corrosion [27]. The localized corrosion originates from Mg_2Pb phases which accelerate the dissolution of as-rolled Mg-6Al-7Pb Alloy. However, the curve of as-rolled Mg-6Al-7Pb-0.3Ce alloy has another inductive loop (R_2, L_2) at low frequency, as remarked in Fig. 9a, and

the inductive loop is associated with Al_4Ce phases according to Fig.6d. Thus, equivalent circuits of the two EIS are fitted with b1 and b2, respectively. In addition, the EIS data in Table 4 are fitted with Zsimpwin software and the fitting equivalent circuits are close to the experimental ones in view of small χ^2 values about 10^{-3}. Generally, the R_t can reflect the discharge activity of the anode material [28]. Thus, as-rolled Mg-6Al-7Pb-0.3Ce alloy shows stronger discharge activity than as-rolled Mg-6Al-7Pb alloy, and Al_4Ce phases can greatly enhance the discharge activity of the Mg-6Al-7Pb-0.3Ce alloy.

3.2.5 Corrosion morphology and anode efficiency

To clarify the discharge process of two experimental alloys, their corroded surfaces after discharging at 200 $mAcm^{-2}$ for 10 s are observed using SEM in Fig. 10. In Fig. 10a, as-rolled Mg-6Al-7Pb alloy suffers severe attack with big pits of which the size is about 20~50 μm, and these pits occurs in the vicinity of Mg_2Pb phases. Apart from big pits, many small pits of which the size is 1~10 μm appear on the surface of as-rolled Mg-6Al-7Pb-0.3Ce alloy. According to Fig. 6d and Fig.10b, the big pits stem from Mg_2Pb phases, while small pits come from the dropping of Al_4Ce because of self-corrosion. This phenomenon is agreement with the result of EIS in Fig.9, because of the synergistic effect of the dispersive Al_4Ce and Mg_2Pb phases. After discharged at 200 mA cm^{-2} for 1200, corroded morphologies of two experimental alloys are shown in Fig. 10c and d, respectively. With 20% CrO_3 solution removing corrosion products formed on the surface of as-rolled alloys, as-rolled Mg-6Al-7Pb-0.3Ce alloy exhibits more uniform corroded morphology compared with as-rolled Mg-6Al-7Pb alloy. When discharge measurements are performed for 1 h, the anode efficiency of as-rolled Mg-6Al-7Pb-0.3Ce alloy is 46.3% at the density of 10 $mAcm^{-2}$ and 85.5% at 200 $mAcm^{-2}$, respectively. The good discharge performance of as-rolled Mg-6Al-7Pb-0.3Ce alloy is attributed to fine grains and Al_4Ce phases. Dispersive Al_4Ce and Mg_2Pb phases coupling with Mg matrix form micro galvanic cells and this process can release hydrogen to promote the dropping of corrosion products and to reduce the electrochemical polarization of alloy surface. However, a part of Mg matrix, which is not involved in the dissolution reaction and the self-corrosion reaction, drops from the alloy matrix. So, the anode efficiency of Mg alloys is lower than 100%. Compared with as-rolled Mg-6Al-7Pb alloy, as-rolled Mg-6Al-7Pb-0.3Ce alloy has finer grains according to Fig.6a and b. The grain refinement can decrease the loss of un-reacted matrix, which is concluded from the previous reports [2, 6, 9]. The grain refinement also increases the number of grain boundaries so as to enhance the electrochemical activity. Therefore, as-rolled Mg-6Al-7Pb-0.3Ce alloy provides higher potential and anode efficiency than as-rolled Mg-6Al-7Pb alloy at different current densities.

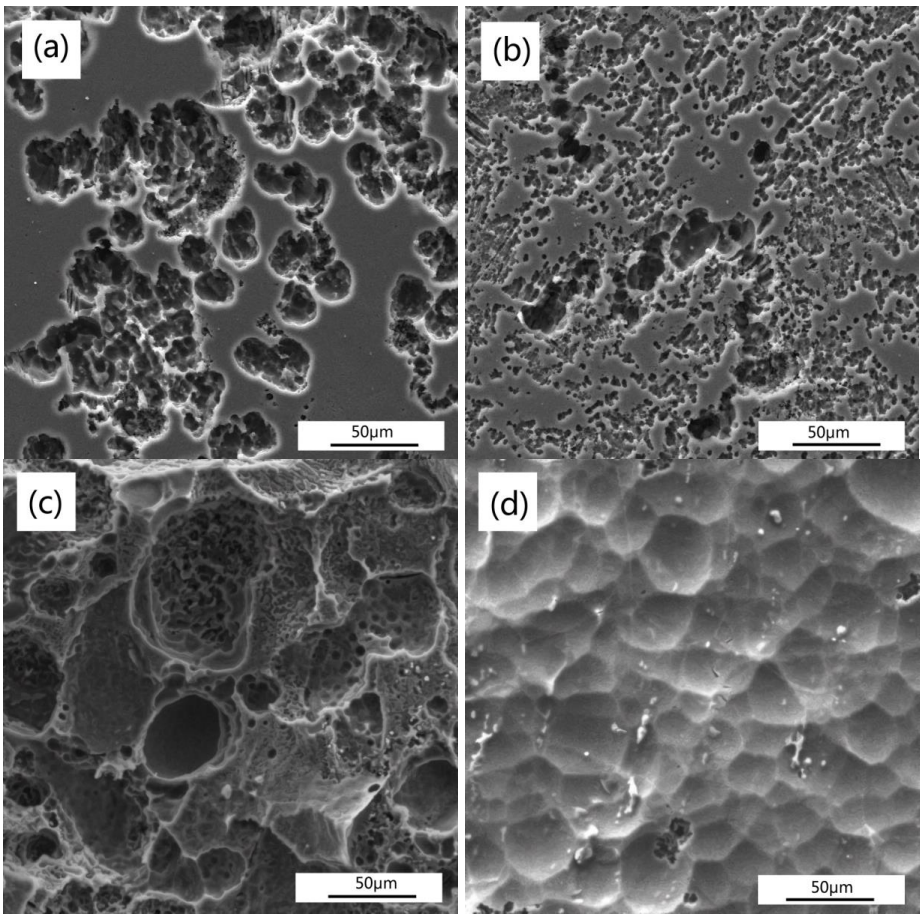

Figure 10. Secondary electron (SE) images of the two as-rolled alloys discharged at 200 $mAcm^{-2}$ for different time, Mg-6Al-7Pb (a) and Mg-6Al-7Pb-0.3Ce (b) for 10 s, Mg-6Al-7Pb (c) and Mg-6Al-7Pb-0.3Ce (d) for 1200 s.

3.2.6 Discharge performance of assembled Mg-air battery

As-rolled Mg-6Al-7Pb-0.3Ce and Mg-6Al-7Pb alloys are adopted as the anodes to assemble Mg-air primary batteries. Fig. 11 shows discharge performances of Mg-air batteries based on the three anodes during different applied current densities. Obviously, the cell based on the Mg-6Al-7Pb-0.3Ce anode shows higher operating voltage at different applied current densities. Moreover, its peak power density reaches 102.7 $mW \cdot cm^{-2}$ at the impress current density of 120 mA cm^{-2}, which is higher compared with those of Mg-Al-Pb-In and Mg-Al-Sn anodes under a similar discharge condition [9, 29]. Therefore, the Mg-6Al-7Pb-0.3Ce alloy with excellent discharge performance has the potential application value in Mg-air battery.

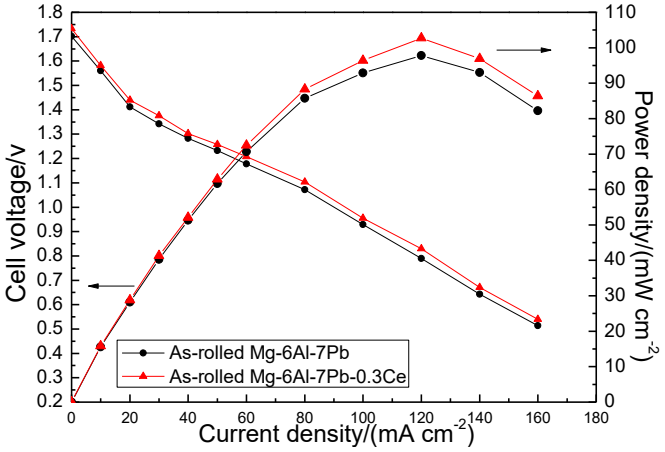

Figure 11. Performance comparison of Mg-air batteries with as-rolled Mg-6Al-7Pb-0.3Ce and Mg-6Al-7Pb alloyanodes.

4. CONCLUSIONS

This study investigates the corrosion behavior and discharge performance of as-cast Mg-6Al-7Pb alloys with different Ce contents. It has been found that the discharge performance of as-cast Mg-6Al-7Pb alloy can be enhanced by adding 0.3% Ce. The discharge property of Mg-6Al-7Pb-0.3Ce alloy is further improved by multi-pass hot rolling. The result is verified by polarization test and electrochemical impedance spectroscopy. Al_4Ce phase has the benefit to inhibit grain growth during multi-pass hot rolling and the uniform microstructure is obtained in as-rolled Mg-6Al-7Pb-0.3Ce alloy. The improved discharge performance of as-rolled Mg-6Al-7Pb-0.3Ce alloy is attributed to the synergistic effect of Al_4Ce phases, Mg_2Pb phases and small grains. The assembled Mg-air battery with as-rolled Mg-6Al-7Pb-0.3Ce alloy as anode also provides higher specific energy (102.7 $Whkg^{-1}$) than these in previous reports. As a result, as-rolled Mg-6Al-7Pb-0.3Ce alloy can be an excellent anode material for Mg-air battery.

ACKNOWLEDGEMENT
This work was financially supported by the Fundamental Research Funds for the Education Department of Hunan Province (17A019, 15C0116), China. The authors also acknowledge the Project (K1705055) supported by the science and technology program of Changsha.

References

1. R. Renuka, *Mater. Chem. Phys*., 59 (1999) 42.
2. J. Li, K. Wan, Q. Jiang, H. Sun, Y. Li, B. Hou, L. Zhu, M. Liu, *Metals*, 6 (2016) 65.
3. N. Wang, R. Wang, C. Peng, C. Hu, F. Yan, P. Bing, *Trans. Nonferrous Met. Soc. China*, 24 (2014) 2427.
4. N. Wang, R. Wang, C. Peng, Y. Feng, X. Zhang, *Trans. Nonferrous Met. Soc. China*, 20 (2010) 1403.
5. N. Wang, R. Wang, C. Peng, Y. Feng, *Corros. Sci*., 81 (2014) 85.
6. N. Wang, R. Wang, C. Peng, Y. Feng, B. Chen, *Corros. Sci*., 64 (2012) 17.

7. L. Wen, K. Yu, H. Xiong, Y. Dai, S. Yang, X. Qiao, F. Teng, S. Fan, *Electrochim. Acta*, 194 (2016) 40.
8. D. Wang, S. Yang, X. Liu, J. Duh, C. Wang, *Mater. Chem. Phys*., 171(2016) 227.
9. N. Wang, R. Wang, C. Peng, B. Peng, Y. Feng, C. Hu, *Electrochim. Acta*, 149 (2014) 193.
10. W. Ping, L. Jianping, G. Yongchun, Y. Zhong, X. Feng, W. Jianli, *Rare Metal Mat. Eng*., 41 (2012) 2095.
11. D. Cao, L. Wu, Y. Sun, G. Wang, Y. Lv, *J. Power Sources,* 177 (2008) 624.
12. Y. Ma, N. Li, D. Li, M. Zhang, X. Huang, *J. Power Sources*, 196 (2011) 2346.
13. B. Lv, J. Peng, Y. Peng, A. Tang, *J. Magn. Alloy*., 1 (2013) 94.
14. W. Li, H. Zhou, P. Lin, S. Zhao, *Mater. Charact*., 60 (2009) 1298.
15. H. Xiong, H. Zhu, J. Luo, K. Yu, C. Shi, H. Fang, Y. Zhang, *J. Mater. Eng. Perform*., 26 (2017) 2901.
16. M.C. Lin, C.Y. Tsai, J.Y. Uan, *Corros. Sci*., 51 (2009) 2463.
17. S.F. Liu, B. Li, X.H. Wang, W. Su, H. Han, *J Mater. Process Tech.*, 209 (2009) 3999.
18. G. Song, Adv. Eng. Mater., 7 (2005) 563.
19. M. Zhao, P. Schmutz, S. Brunner, M. Liu, G. Song, A. Atrens, *Corros. Sci.*, 51 (2009) 1277.
20. Y. Fan, G. Wu, C. Zhai, *Mat. Sci. Eng*. A, 433 (2006) 208.
21. H. Zhao, P. Bian, D. Ju, *J. Environ. Sci*., 21 (2009) S88.
22. L. Fan, H. Lu, J. Leng, *Electrochim. Acta*, 165 (2015) 22.
23. S. Candan, M. Unal, M. Turkmen, E. Koc, Y. Turen, E. Candan, *Mat. Sci. Eng*. A, 501(2009) 115.
24. M. Ben-Haroush, G. Ben-Hamu, D. Eliezer, L. Wagner, *Corros. Sci*., 50 (2008) 1766.
25. M. Bai, Y. Sun, Y.H. Duan, *Corrosion Engineering, Science and Technology*, 50 (2015) 34.
26. X. Zhang, H. Wang, *J. Mater. Eng. Perform*., 25 (2016) 1122.
27. Y. Song, D. Shan, R. Chen, E. Han, *J. Alloy Comp*., 484 (2009) 585.
28. F. Yan, R. Wang, C. Peng, H. Tang, H. Liu, *Progress in Natural Science: Materials International*, 21 (2011) 73-79.
29. H. Xiong, K. Yu, X. Yin, Y. Dai, Y. Yan, H. Zhu, *J. Alloy Compd*., 708 (2017) 652.